scientific reports

Check for updates

OPEN

The effects of surface termination, stoichiometry, and strain on the optical properties of bulk-like ZnSe/ZnS core–shell nanocrystals

Michał Zieliński[1]✉ & Agnieszka Gajewicz-Skretna[2,3]✉

Blue-emitting, cadmium-free quantum dots are increasingly vital for optoelectronic applications such as displays and bio-tagging. In particular, bulk-like ZnSe nanocrystals and core–shell quantum dots—with a thin ZnS shell on a ZnSe core—have emerged as promising candidates for blue-light emission. In this study, we employed an atomistic tight-binding approach to investigate these systems. We examined the influence of anion-cation stoichiometry, with particular emphasis on surface termination, and assessed the effect of shell growth on single-particle and excitonic spectra. Our findings revealed significant spectral differences among dots of nominally identical composition, arising from subtle variations in the anion-cation balance. Notably, we demonstrated that strain in large ZnSe/ZnS nanocrystals induces a blueshift in the emission energy, contrary to the conventional expectation of a redshift. These results provide valuable insights into the spectral engineering of heavy-metal-free quantum dots via precise tailoring of core–shell dimensions.

Keywords Quantum dots, Core/shell nanocrystals, ZnSe/ZnS, Atomistic empirical tight-binding method, Spectral properties, Electronic properties, Band gap energy

The search for environmentally benign and efficient light-emitting materials has accelerated research into cadmium-free quantum dots. In optoelectronics, blue-emitting quantum dots are essential for next-generation displays, solid-state lighting, and bio-imaging applications[1,2]. Among various material systems, ZnSe nanocrystals and ZnSe/ZnS core–shell structures have garnered considerable attention due to their favorable optical properties and inherent chemical stability[3]. Combining a ZnSe core with a thin ZnS shell not only passivates surface states but also enables the tunability of emission wavelengths through controlled strain and interfacial effects[4,5]. Bulk-like nanocrystals[6]exhibit unique characteristics due to their increased volume and altered surface-to-volume ratio. Hence, the interplay between surface stoichiometry, structural strain, and shell growth becomes particularly critical in these systems. Variations in the anion-cation balance at the surface can significantly alter the electronic structure, leading to pronounced differences in single-particle and excitonic spectra[7,8]. Moreover, while strain is conventionally associated with redshifts in emission energies, recent observations suggest that strain may induce a blueshift in large ZnSe/ZnS nanocrystals[3,6].

In this work, we systematically explore these phenomena using an atomistic tight-binding framework. By rigorously analyzing the effects of surface termination, stoichiometric variations, and strain, we aim to elucidate the underlying mechanisms governing the optical response of these heavy-metal-free quantum dots. Our study enhances the fundamental understanding of core–shell nanostructures and lays the groundwork for advanced spectral engineering, thereby contributing to the development of more efficient, cadmium-free optoelectronic devices.

Recently, extensive research has been conducted on heavy-metal-free nanocrystals based on ZnSe and ZnSe/ZnS core–shell nanocrystals[3,6,9–13]. These studies have focused on the synthesis of high-quality, large (or very large), stable quantum dots with good optical properties, preferably with narrow emission lines and high-fluorescence quantum efficiency, and, most importantly, with emission peaks in the blue-emitting region. Large quantum dot sizes enable an emission shift in the desired spectral region and suppress undesired Auger recombination and

[1]Institute of Physics, Faculty of Physics, Astronomy, and Informatics, Nicolaus Copernicus University, Toruń, Poland. [2]Department of Physical Chemistry, Faculty of Chemistry, Gdansk University of Technology, Gdansk, Poland. [3]Laboratory of Environmental Chemoinformatics, Faculty of Chemistry, University of Gdansk, Gdansk, Poland. ✉email: mzielin@fizyka.umk.pl; agnieszka.gajewicz-skretna@pg.edu.pl

Förster resonant energy transfers in packed quantum dot films[6]. From a theoretical viewpoint, these systems also present a formidable challenge. For example, a 10 nm ZnSe quantum dot with a two-monolayer-thick ZnS shell will have the number of atoms reaching 45×10^3. This number will rapidly increase with further size increases, as the number of atoms grows to the third power as a function of the nanocrystal radius reaching 200×10^3 atoms in 18 nm diameter ZnSe nanocrystals (such as studied experimentally by Long et al.[13]). Despite the growth of computational power, such numbers of atoms are typically prohibitive for density functional theory (DFT)-based methods[14].Moreover, the DFT often faces significant challenges when calculating band gaps (and thus emission energies/wavelengths) even when using hybrid potentials or DFT + U approaches[15]. Here, we use the atomistic empirical tight-binding method, which has proven its applicability for various small and large nanostructures[16–18]. The tight-binding was then followed by exact diagonalization (configuration interaction) and many-body calculations, which are essential for predicting a nanostructure's excitonic properties (emission energy/wavelength)[19].

We begin by studying a family of spherical ZnSe nanocrystals as a function of their size. We focus on the anion-cation balance that comes from either the choice of the center of the nanocrystal with respect to the crystal lattice or from the surface-termination (i.e., Zn or Se-terminated surfaces), with only the type of ionic species residing on the surface. We demonstrate that, due to the large surface-to-volume ratio of these nanocrystals, this effect plays a vital role in their spectra. For comparison (see Supplementary Information), we performed the same calculation for CdSe and ZnS nanocrystals and obtained similar conclusions. Our theoretical results for core-only ZnSe nanocrystals agree with recent experimental observations and may be used to better understand the notable disparities between different experimentally measured systems. Next, we focus on the role of shells, and, in particular, we show that for small ZnSe core nanocrystals, the addition of the ZnS shell lowers (redshifts) the emission energy due to decreased confinement. However, the shell has a less-than-expected effect on the emission energy of large core systems, where it increases (blueshifts) the emission energy due to strain.

Results

Figure 1 schematically shows the ZnSe/ZnS core–shell nanocrystals of interest. Please note the broad range of diameters (D), from very small up to very large nanocrystals (as studied, e.g., in Long et al.[13]). We began our analysis using cases with zero shell thickness (H = 0), corresponding to uncapped (core-only) nanocrystals. We also studied uncapped CdSe and ZnS nanocrystals for comparison (see Supplementary Information).

In atomistic calculations, nanocrystals are defined as a spherical cut from an underlying crystal lattice. There are multiple ways in which the sphere (nanocrystal) shape can be carved from a crystal lattice, resulting in a different stoichiometry. In the tight-binding calculation, there are three natural choices for choosing the center of the coordinate system, that is, the center of the quantum dot[20]. This could be at an anion, a cation, or the midpoint of a bond between an anion and a cation. In this work, we tested all three possibilities. For anion-centered (A) or cation-centered (C) dots, this led to unequal numbers of anions (N_a) and cations (N_c); however, spherical dots centered at the mid-bond (M) had an equal number of anions and cations. This is illustrated in Fig. 2 as the $\frac{(Na-Nc)}{(Na+Nc)}$ ratio may vary profoundly (for A and C cases) depending on size. This effect was particularly notable for small nanocrystals with a large surface-to-volume ratio (as shown in the inset in Fig. 2 (**a**)). For the same reason, the ionic imbalance was especially strong on the nanocrystal surface (i.e., those atoms with passivated dangling bonds, as illustrated in Fig. 2 (**b**)), where only surface atoms were taken into consideration.

In some experiments[12], the surface may consist of only one type of ionic species (e.g., a Zn-surface or a Se-surface). To account for this, we can mimic the surface treatment in models by removing surface atoms of a given kind. This process leads to anion-only or cation-only terminated surfaces. Such cases are shown in Fig. 2 by using

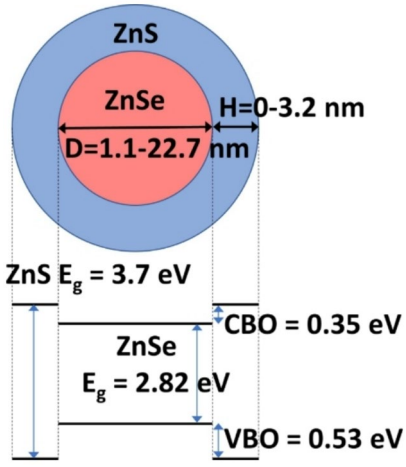

Fig. 1. Schematics of the geometry and band alignment for ZnSe core/ZnS shell systems under consideration with D core diameter and H shell thickness (H = 0 corresponds to pure ZnSe (core-only) nanocrystals. CBO and VBO correspond to conduction and valence band offset, respectively.

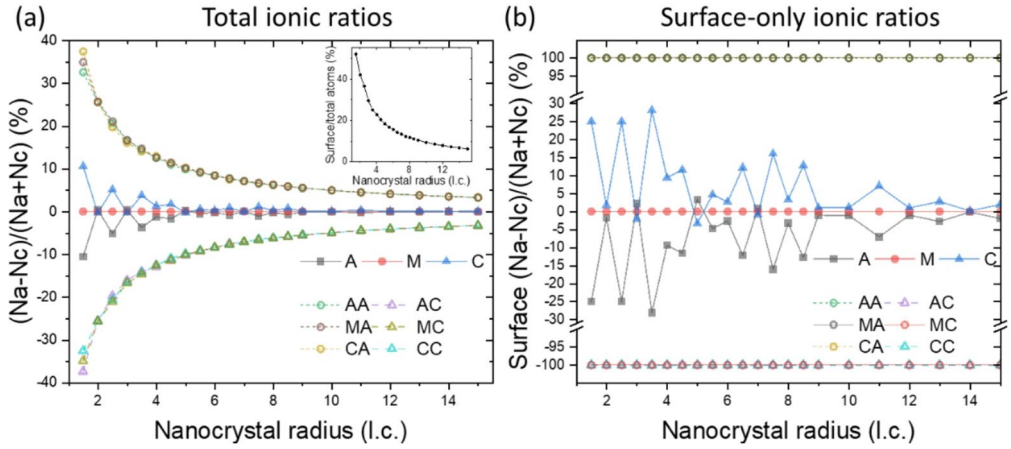

Fig. 2. Ionic ratios (in %) were calculated using numbers of anions (Na) and cations (Nc) present in spherical nanocrystals of different radii (in lattice constants) cut from a zinc-blende crystal lattice using different atoms as the origin of the coordinate system (A - anion, C - cation, M - midpoint), as well as by terminating the surface with one of ionic species (these cases are marked using a double letter notation, e.g., AC corresponds to the anion in the center of the coordinate nanocrystal and the cation-terminated surface). Plot (**a**) includes all atoms in the nanocrystals, whereas (**b**) shows results for surface atoms only. The inset in (**a**) shows the overall ratio of surface atoms to the total number of atoms as a function of size. Please note the substantial stoichiometric variations in several cases. As shown in (**b**), for a fully anion-terminated surface (AA, MA, CA) or a cation-terminated surface (AC, MC, CC), all surface atoms were either anions or cations, respectively, by definition.

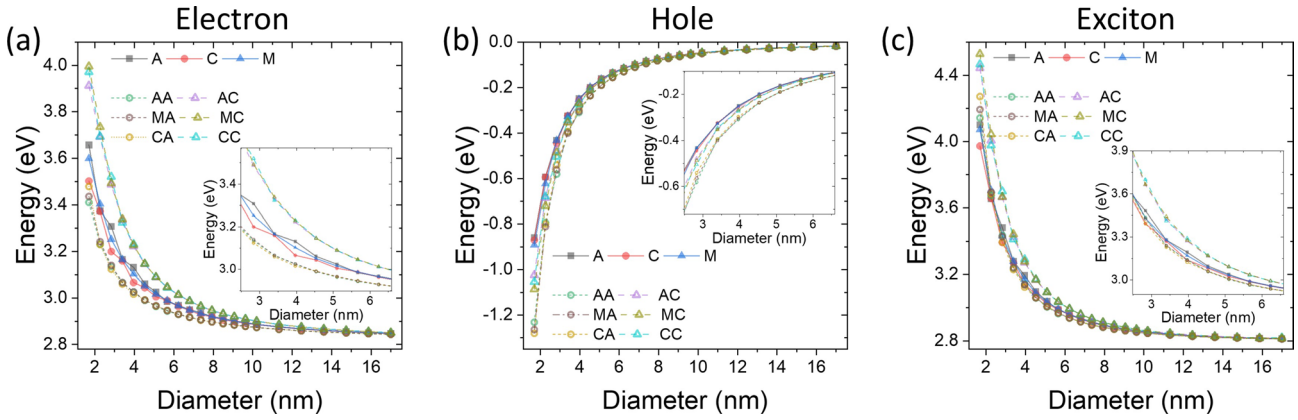

Fig. 3. Ground electron and hole states, as well as the excitonic ground state energy as a function of diameter for ZnSe nanocrystals. Nanocrystals were cut from the crystal lattice by placing the origin at different points (A - selenium anion, C- zinc cation, M - mid-point; see text for more) and/or terminated with one ionic species only (second letter in a double letter notation: A - selenium, C - zinc). Insets magnify the low-diameter ranges. Please note the substantial variations depending on the stoichiometry.

a double letter notation, where the first letter stands for the dot center (A, C, M), and the second letter describes the type of surface (A for anion-terminated, C for cation-terminated). For example, for ZnSe nanocrystals, AC stands for the dot center on Se (anion) with a Zn-terminated surface.

As the volume-to-surface ratio is large at the nanoscale, surface treatment leads to a strongly unbalanced stoichiometry of the entire nanocrystal (Fig. 2 (a)), even for larger diameters. We noted that for anion- and cation-terminated cases, the surface itself (by definition) was occupied by one type of ionic species only (as confirmed by 100% ratios in Fig. 2 (a)).

The compositional variation affects both single particle and many-body spectra of ZnSe nanocrystals, as shown in Fig. 3. For small nanocrystals (with larger surface/volume ratios), the electron ground state varied on the scale of hundred meVs, with the Zn cation-terminated case forming an 'upper bound' for electron ground state energy. In contrast, Se anion-terminated cases appeared to limit these electron energies from below. Cases with a mixed surface (A, C, M) appear in the center of the scale, with some notable fluctuations on the top distance dependence (see the inset in Fig. 3(a)). The dispersion of the results was substantial (≈0.1 eV), even for relatively large diameters (6–8 nm). For the hole (Fig. 3(b)), a similar effect was observed; however, there

was less variation than for electrons due to stronger hole confinement. Moreover, for the hole, anion-terminated (AA, MA, CA) cases appear to have the lowest energies, and cation-terminated (AC, MC, CC) cases were in the middle of the spectrum. In contrast, mixed anion/cation surfaces (as it happened for A, C, and M) appear to limit the hole spectrum from the top.

Overall, electron and hole dependence based on stoichiometry must also be reflected in the spectra of interacting electron-hole pairs, i.e., exciton, as shown in Fig. 3(c). In general, Zn-cation-terminated cases have higher emission energies than Se-anion-terminated cases, with the energy difference ranging from 0.3 eV for small (3 nm) nanocrystals to dozens of meVs for mid-sized systems. This is consistent with recent experimental observations[12], where a pronounced (although smeared) redshift in absorption spectra is observed for Se-terminated ZnSe quantum dots compared to Zn-terminated systems. Lin et al.[12] also show results for CdSe; therefore, for completeness, we performed similar calculations for CdSe nanocrystals (see Supplementary Information Fig. S1). We found that, again, Se-anion-terminated nanocrystals have their excitonic energies redshifted with respect to the Cd-cation-terminated cases. That is, for a 4.8 nm diameter system, Cd-terminated nanocrystals have an emission energy of ≈ 1.98 eV, compared to Se-terminated surfaces of ≈ 1.89 eV, corresponding to emission wavelengths of 626 nm and 656 nm, respectively. Similar spectral differences were observed in the experiment by Lin eta al[12]. We also noted that a substantial dependence on stoichiometry could also be found for ZnS nanocrystals (see Supplementary Information Fig. S2). Finally, we observed that with sizes larger than 10 nm, the role of surface (as well as the total) stoichiometry starts to play a negligible role in excitonic emission energy, as well as for electron and hole ground states energies, due to a smaller surface/volume ratio.

Different stoichiometric choices mimic variations that can occur (deliberately or not) in experiments. Figure 4 compares the results of our calculations (with the AA variant) with recent experimental results (shown as data points from four separate experiments and as three experimental fits (curves)). As nanocrystal experiments are often performed at room temperature, we performed additional TB calculations for ZnSe with a room temperature (2.7 eV) band gap set in the tight-binding parametrization (see Methods). Our results agreed with the experimental ones, although we noted a pronounced difference between the various experimental results reported[13]. These may be due to different growth modes (leading to slight variations in size, shape, and composition) and measurement conditions (e.g., temperature). We also noted that these curves, provided by fitting to a particular experiment, are often fit only in a specific range of nanocrystal sizes and, thus, may have poor asymptotic behavior (e.g., underestimating bulk band gaps in the limit of very large nanocrystals). Considering all the above factors, we concluded that our approach aligns well with the experimental results.

core–shell

Thus far, we have discussed core-only systems; in the following, we discuss ZnSe/ZnS core–shell nanocrystals as a function of core–shell diameter and thickness. For type-I confinement, as in the ZnSe/ZnS system (see band alignment in Fig. 1), the role of the shell is to separate the core surface from its surrounding environment[21]. Thus, one would expect a small effect of shell (and overall) surface stoichiometry on the excitonic spectra. As shown in Fig. 5, for small (2.7 nm) and medium (5.7 nm) nanocrystals, 1 nm (2 lattice constants) ZnS shells strongly suppress excitonic energy variations due to stoichiometry. In Fig. 5, we compared several select cases (A, AA, AC) for clarity; however, we found similar results for all other stoichiometric choices (M, C, MA, MC, CA, CC). We also performed a systematic analysis (between A and AA) for all core diameters and shell thicknesses considered in this work (see Supplementary Information Fig. S3). In all cases, we found that there were substantial (> 50 meV) differences due to stoichiometry, primarily for small (< 4 nm) core diameters and small (< 1.5 nm) shell thicknesses. Notably, minor (< 10 meV) differences between different stoichiometric realizations were still present, even in the largest nanocrystals.

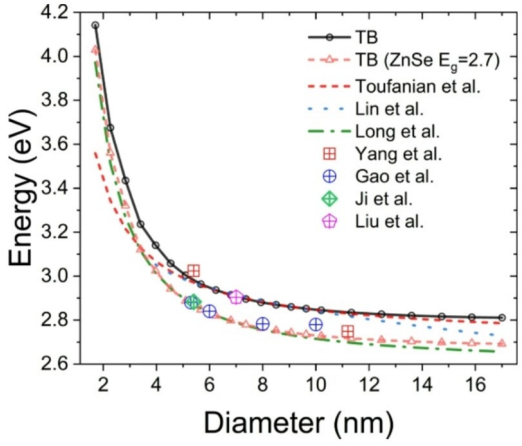

Fig. 4. A comparison of the excitonic ground state energy as calculated in this work–TB, anion-centered with anion (sulfur) terminated surface–and as reported by other authors, either via experimental data points or functions fit to the experiment. "TB ZnSe (E_g=2.7 eV)" corresponds to a tight-binding calculation using a ZnSe (room-temperature) energy band gap of 2.7 eV.

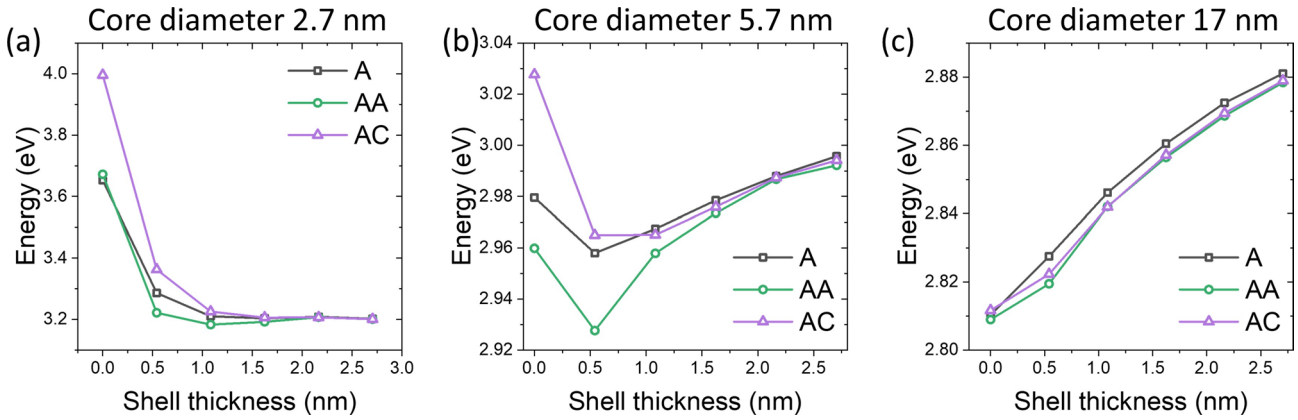

Fig. 5. Excitonic ground state energy as a function of shell-thickness calculated for three nanocrystals of different sizes and three possible stoichiometric choices. Note different energy scales, overall trends, and weak stoichiometry dependence for large core/shell sizes.

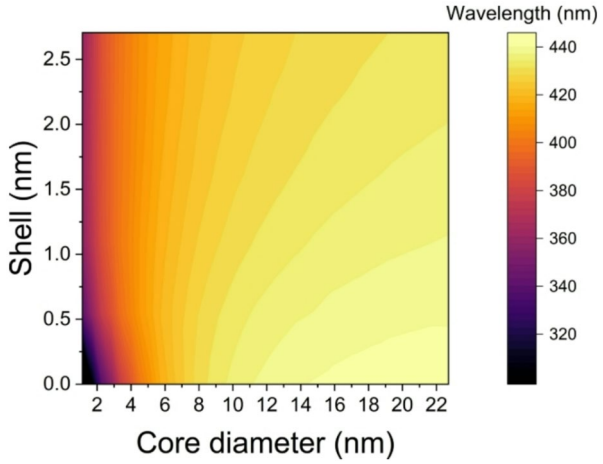

Fig. 6. The excitonic energy wavelength as a function of ZnSe core diameter and ZnS shell thickness. For small core diameters, there is a weak redshift with increasing shell thickness. However, for large core diameter cases, there is a blueshift with increasing shell thickness.

Apart from stoichiometric differences, Fig. 5 reveals interesting trends related to shell thicknesses. For a small (2.7 nm) core diameter, adding a shell would substantially reduce (on the order of 0.5 eV) the excitonic emission energy. This effect was expected[21], as the shell, despite a larger band gap, effectively increases the overall quantum dot size, thereby reducing confinement. A similar effect was also present for the 5.7 nm dot. However, for the 5.7 nm case, the larger shell thickness (> 1.0 nm) increases the emission energy. Moreover, it is apparent that adding a shell increases the emission energy for larger quantum dots rather than lowering it. This effect appeared to persist for all large-core diameters (as shown in Fig. 6), where we show the emission wavelength as a function of core/shell dimension and, for one (A), choice of stoichiometry. As apparent from the plot, for small-core diameters only, the incorporation of the shell increases the emission wavelength (i.e., decreases the energy). There was an intermediate region where the shell weakly affected the emission wavelength, whereas for larger dots (say > 8 nm), the addition of the shell increased the emission wavelength instead of lowering it.

This blueshift effect, caused by ZnS capping in large ZnSe nanocrystals, was recently observed experimentally (Ji et el[3]. and Gao et al.[6]) and was attributed to strain effects. For further comparison with the experiments, we used a low-temperature band gap, as given in the tight-binding parametrization. A fair comparison with the experiment performed at room temperature shows a reduction in emission energies of 0.1 eV. That is, it increases the emission energy from ≈ 440 nm to ≈ 460 nm, consistent with experimental observations.

To justify claims regarding strain reported in experimental papers, we performed a series of calculations for the anion-centered dots (A) on the excitonic emission energy with strain effect accounted for or artificially neglected, as shown in Fig. 7. For small dots, the addition of a shell reduces (redshifts) the excitonic energy. For dots with a diameter of 5.7 nm (and larger), adding more than 1 nm of shell thickness results in a blueshift of energy in the strained case. Similarly, adding any ZnS shell for a larger dot diameter systematically increases excitonic energy. This effect was, however, absent without strain included in the calculation (Fig. 7(b)), where

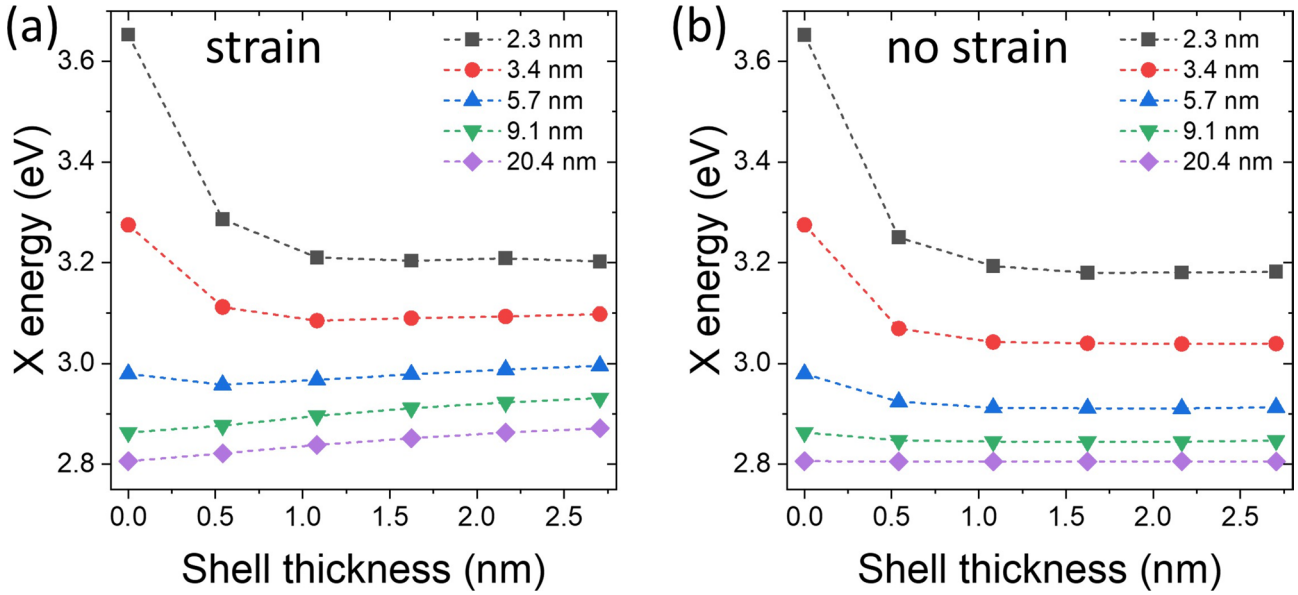

Fig. 7. Excitonic ground state energy calculated **a** with strain (ZnSe/ZnS lattice-mismatch) included in the calculation and **b** the strain artificially neglected, and as a function of shell thickness for several nanocrystals of different core diameters. Please note that different trends were observed for larger core diameters due to strain effects.

the addition of the shell always reduced the emission energy or did not affect it at all (in large dots). Thus, the overall effect was an apparent interplay between decreased confinement due to the shell (redshifting energy) and increased compressive strain (blueshifting energy). These two effects combine differently depending on core/shell sizes, as discussed below.

In Fig. 8, we further investigated the evolution of electron and hole single-particle ground state energies (which form the exciton) and the degree of their localization in the core area. For a small (2.3 nm) dot, there is an overall monotonic decrease/increase of electron/hole energies when adding shell thicknesses, thus effectively reducing the single-particle gap (e1-h1). The difference between cases with strain included and those without was generally only quantitative. For this size, either the electron or hole (strained or not) tends to delocalize more into the shell area (or less in the core) with increasing shell thickness, effectively reducing their confinement (see also Supplementary Information Fig. S4-S5 for further strain plots, and Fig. S6-S7 for selected radial density plots).

For a medium-sized (5.7 nm) dot, there is a significant difference between electron state evolution when strain is included or neglected. The inclusion of strain increases the electron energy rather than lowering it. The shell imposes a compressive strain on the core, which, through the a_c deformation potential, shifts the energy up at the bottom of the conduction band; thus, increasing the electron energy. The more shell material, the larger the strain, with the shift increasing with shell thickness. The effect was so substantial that, for the electron, it dominated the simultaneous reduction of confinement. This contrasts with the hole, which still resembles the behavior characteristic of the smaller system. As the core was larger (5.7 nm), both the electron and hole tend to penetrate the shell less than in the small (2.35 nm) nanocrystal case (note the different vertical scales in Fig. 8(d) and (e)). Nonetheless, for the medium-sized dot, when comparing the degree of charge localization between strained and unstrained cases, we noticed a more significant degree of core localization in the latter.

This indicates that tensile strain in the shell (and compressive strain in the core) effectively lowers the ZnSe/ZnS valence and conduction band offsets compared to unstrained cases. (We note here that in ZnSe/ZnS spherical nanocrystal, the core is under hydrostatic compressive strain, with no biaxial strain component, whereas the shell is under tensile, biaxial strain. The hydrostatic component of tensile strain in the shell effectively lowers the confining potential profile for the electron in the shell or, in other words, effectively reduces the ZnSe/ZnS conduction band offset. As there is no biaxial strain in the core, there is no heavy-hole/light-hole strain splitting component in the core region. Contrarily, the shell is under a substantial biaxial strain, which splits light- and heavy-hole. This effectively reduces the valence band offset, although only for light holes, allowing the hole to penetrate deeper into the shell.)

The role of strain is even more pronounced for the largest quantum dot (20.4 nm) we considered. The electron is monotonously blue-shifted with increasing strain due to increasing shell thickness, while its charge density is mostly pinned to the core. In contrast, the hole tended to migrate slightly deeper into the shell. Overall, for the hole in the large system, we observe a very weak effect of strain on its energy as the strain contribution cancels energy shifts due to confinement (see also Supplementary Information Figs. S8-S10 for qualitative comparison with the effective mass approach).

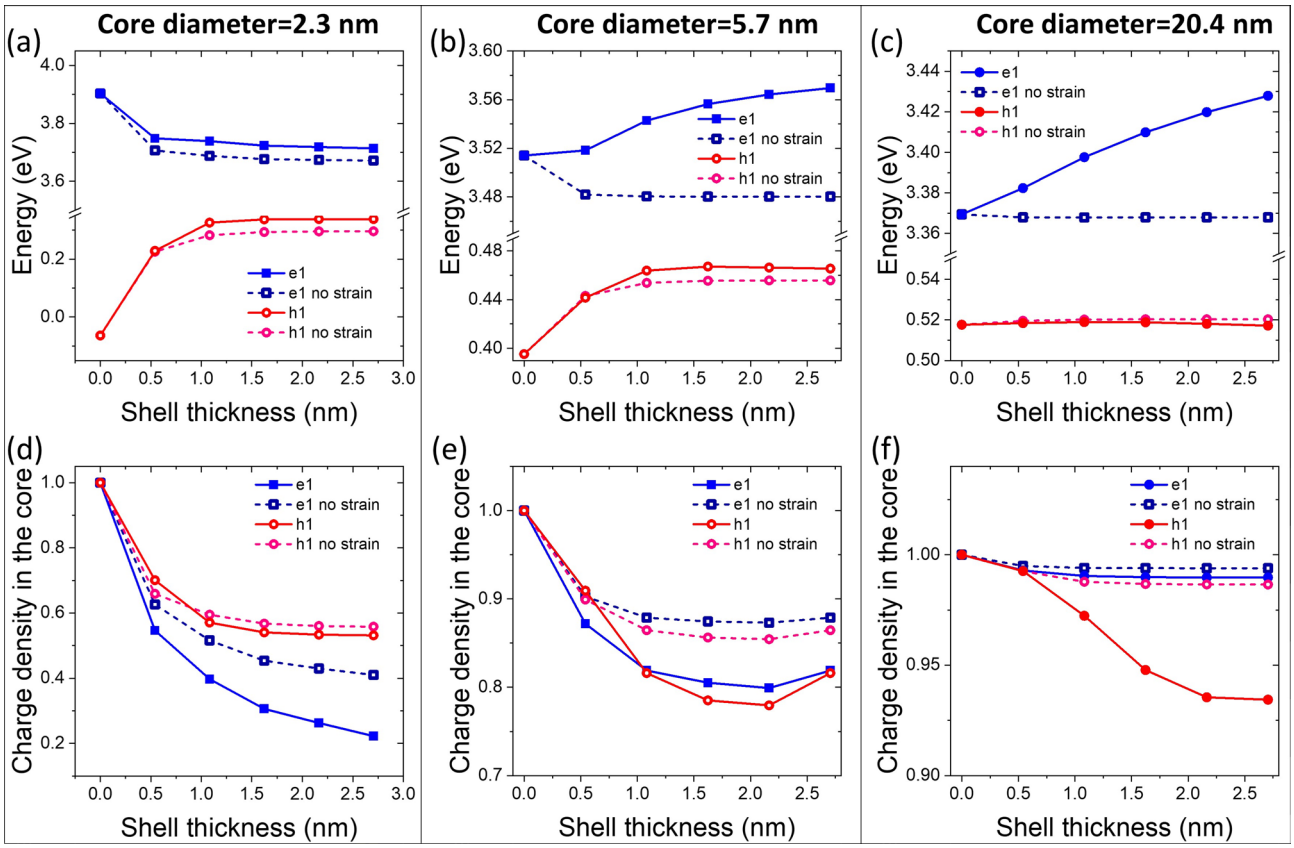

Fig. 8. **a-c** Single particle electron and hole ground state energies and **d-f** degrees of their localization in the nanocrystal core as a function of ZnS shell thickness for three nanocrystals of different ZnSe core diameters. Results obtained with the strain included in the calculations were compared with those with the strain artificially neglected. Note the different vertical scales on each of the plots.

Methods

For the calculations of nanocrystal energy spectra, we used the empirical tight-binding method within the sp^3s^*model[22], with parameters fitted to reproduce bulk properties, such as the band gap (from Lippens and Lannoo[17], and augmented to account for spin-orbit interactions[23]. Additionally, for ZnSe (when specified in the text), we modified the tight-binding parameters related to the bottom of the conduction band to account for the decreased bulk band gap at room temperature. The valence band offset between ZnSe and ZnS (0.53 eV) was taken from Wei and Zunger[24], and it is consistent with other theoretically reported values (e.g. 0.52 eV from Li et al.[25] or 0.58 eV from Van de Walle[26]. There was a substantial 4.5% mismatch between the ZnSe/ZnS lattice constants (i.e., 0.5667 nm for ZnSe vs. 0.541 nm for ZnS); therefore, to account for strain, we used the valence-force field method of Keating[27] with parameters taken from Martin[28]. We used the conjugate gradient method to find the position of atoms that minimized strain (optimize geometry), assuming free (open) boundary conditions, allowing for surface relaxation. We then performed empirical tight-binding calculations for these optimized atomic positions, using the Arnoldi sparse solver as implemented in ARPACK[29] to find several lowest electron and hole states, including the ground hole and electron states. Strain was included in the Hamiltonian via Slater-Koster rules[30] to account for changes in bond angles and via the Harrison law[31] to describe variations of bond lengths. Perfect tetrahedral bond angles and uniform lengths were assumed in cases where strain effects were neglected. To remove spurious states due to dangling bonds, we used the model by Lee et al.[32], where an energy shift is applied to surface bonds instead of modifying the surface atom's energies. This scheme has been widely successful in mimicking the passivation of dangling bonds in a broad family of quantum dots.

After the tight-binding calculations, the excitonic spectra[19] were calculated using the configuration-interaction method described in Zieliński et al.[18]. We perform many-body calculations using a basis set involving eight (with spin) lowest electron and eight (with spin) highest hole configurations (a total of 64 excitonic configurations). However, we found, by comparison, that these results did not significantly vary from the minimal basis set involving two (with spin) lowest electron states and two (with spin) highest hole states. The incorporation of the electron-hole interaction, even at the simplest level, was crucial, as the single-particle (HOMO-LUMO) gap would have strongly overestimated the effective (optical) gap observed experimentally, e.g., by 140 meV for 5.7 nm ZnSe nanocrystals.

Conclusions

In this work, we studied, using an atomistic tight-binding approach coupled with the configuration interaction method, the single-particle and excitonic ground states of multiple ZnSe/ZnS core–shell nanocrystals as a function of size and different stoichiometric choices. Modeling such systems can be challenging due to the substantial number of atoms in the simulations and the peculiarities of anion-cation balance. In experiments, no two quantum dots can be identical. Not only can they differ in size or shape, which leads to an inhomogeneous broadening of their spectra, but they can also have different numbers of anions/cations at nominally identical sizes and/or differently terminated surfaces. However, in theory, one has the freedom to choose a nanocrystal center with respect to the crystal lattice. This choice is arbitrary, and multiple options must be accounted for to avoid the arbitrariness of the simulation. Furthermore, ZnSe nanocrystals can have Zn- or Se-terminated surfaces, which may noticeably affect their spectra, and such cases should also be considered in realistic modeling. The latter may lead to a substantial dispersion of results, which, in turn, can pose challenges when comparing theoretical results with experimental ones. In this regard, our results are in agreement with experimental data, and we further discuss the role of the room-temperature band gap for comparison. We also performed analogous calculations for CdSe and ZnS nanocrystals (see the Supporting Information). Furthermore, we performed a series of challenging computations for core–shell ZnSe/ZnS nanocrystals as a function of core diameter and shell thickness, with strain effects artificially neglected. We concluded that strain plays a vital role in these systems. We found that the addition of a shell redshifts the emission energy in small dots, while in large dots, the strain imposed by the shell increased the excitonic emission energy. This blueshift is not necessarily attributable to the strain-induced interfacial defects resulting from fast shell growth, as suggested by other authors[3], or alloying, as neither of these effects was included in our model. Instead, this is a 'volume' effect that persists even with perfect interfaces without alloying or defects. Finally, we note that atomistic modeling, with the predictive capability of emission energies, is essential when designing novel quantum dots, including large, heavy-metal-free ZnSe/ZnS nanocrystals.

Data availability

The datasets used and/or analysed during the current study are available from the corresponding author on reasonable request.

Received: 26 August 2025; Accepted: 10 February 2026
Published online: 20 February 2026

References

1. Xu, G. et al. New generation cadmium-free quantum dots for biophotonics and nanomedicine. *Chem. Rev.* **116**(12327), 12234. https://doi.org/10.1021/acs.chemrev.6b00290 (2016).
2. Cai, F. et al. Blue quantum Dot light-emitting diodes toward full-color displays: Materials, devices, and large-scale fabrication. *Nano Lett.* **25**, 1–15. https://doi.org/10.1021/acs.nanolett.4c02968 (2025).
3. Ji, B., Koley, S., Slobodkin, I., Remennik, S. & Banin, U. Znse/zns core/shell quantum Dots with superior optical properties through thermodynamic shell growth. *Nano Lett.* **20**, 2387–2395. https://doi.org/10.1021/acs.nanolett.9b05020 (2020).
4. Chen, X., Lou, Y., Samia, A. C. & Burda, C. Coherency strain effects on the optical response of core/shell heteronanostruc-tures. *Nano Lett.* **3**, 799–803. https://doi.org/10.1021/nl034243b (2003).
5. Yang, S., Prendergast, D. & Neaton, J. B. Strain-induced band gap modification in coherent core/shell nanostructures. *Nano Lett.* **10**, 3156–3162. https://doi.org/10.1021/nl101999p (2010).
6. Gao, M. et al. Bulk-like Znse quantum dots enabling efficient ultranarrow blue light-emitting diodes. *Nano Lett.* **21**, 7252–7260. https://doi.org/10.1021/acs.nanolett.1c02284 (2021).
7. Lei, H., Li, J., Kong, X., Wang, L. & Peng, X. Toward surface chemistry of semiconductor nanocrystals at an atomic- molecular level. *Acc. Chem. Res.* **56**, 1966–1977. https://doi.org/10.1021/acs.accounts.3c00185 (2023).
8. Kim, M., Choi, M., Choi, S. & Jeong, S. Semiconductor nanocrystals: unveiling the chemistry behind different facets. *Acc. Chem. Res.* **56**, 1756–1765. https://doi.org/10.1021/acs.accounts.3c00123 (2023).
9. Yang, Z. et al. A seed-mediated and double shell strategy to realize large-size znse/zns/zns quantum Dots for high color purity blue light-emitting diodes. *Nanoscale* **13**, 4562–4568. https://doi.org/10.1039/D0NR05025C (2021).
10. Liu, Y. et al. one-pot synthesis and shape control of Znse semiconductor nanocrystals in liquid paraffin. *J. Mater. Chem.* **20**, 4451–4458. https://doi.org/10.1039/C0JM00115E (2010).
11. Toufanian, R., Zhong, X., Kays, J. C., Saeboe, A. M. & Dennis, A. M. Correlating Znse quantum Dot absorption with particle size and concentration. *Chem. Mater.* **33**, 7527–7536. https://doi.org/10.1021/acs.chemmater.1c02501 (2021).
12. Lin, S. et al. Surface and intrinsic contributions to extinction properties of Znse quantum dots. *Nano Res.* **13**, 824–831. https://doi.org/10.1007/s12274-020-2703-2 (2020).
13. Long, Z. et al. A reactivity-controlled epitaxial growth strategy for synthesizing large nanocrystals. *Nat. Synth.* **2**, 296–304. https://doi.org/10.1038/s44160-022-00210-5 (2023).
14. Martin, R. M. *Electronic Structure: Basic Theory and Practical Methods* (Cambridge University Press, 2020).
15. Perdew, J. P. & Levy, M. Physical content of the exact kohn-sham orbital energies: band gaps and derivative discontinuities. *Phys. Rev. Lett.* **51**, 1884–1887. https://doi.org/10.1103/PhysRevLett.51.1884 (1983).
16. Harrison, W. A. Tight-binding methods. *Surf. Sci.* **299–300**, 298–310. https://doi.org/10.1016/0039-6028(94)90662-9 (1994).
17. Lippens, P. E. & Lannoo, M. Calculation of the band gap for small cds and Zns crystallites. *Phys. Rev. B.* **39**, 10935–10942. https://doi.org/10.1103/PhysRevB.39.10935 (1989).
18. Zieliński, M., Korkusiński, M. & Hawrylak, P. Atomistic tight-binding theory of multiexciton complexes in a self-assembled InAs quantum Dot. *Phys. Rev. B.* **81**, 085301. https://doi.org/10.1103/PhysRevB.81.085301 (2010).
19. Michler, P. (ed) *Topics in Applied Physics* Vol. 90 (Springer, 2003).
20. Little, R. B., El-Sayed, M. A., Bryant, G. W. & Burke, S. Formation of quantum-dot quantum-well heteronanostructures with large lattice mismatch: Zns/cds/zns. *J. Chem. Phys.* **114**, 1813–1822 (2001). https://pubs.aip.org/aip/jcp/article-pdf/114/4/1813/19297859/1813_1_online.pdfDOI: 10.1063/1.1333758.
21. Ghosh Chaudhuri, R. & Paria, S. Core/shell nanoparticles: Classes, properties, synthesis mechanisms, characterization, and applications. *Chem. Rev.* **112**, 2373–2433. https://doi.org/10.1021/cr100449n (2012).
22. Chadi, D. J. & Cohen, M. L. Tight-binding calculations of the valence bands of diamond and zincblende crystals. *Phys. Status Solidi (b)* **68**, 405–419. https://doi.org/10.1002/pssb.2220680140 (1975).

23. Chadi, D. J. Spin-orbit splitting in crystalline and compositionally disordered semiconductors. *Phys. Rev. B.* **16**, 790–796. https://doi.org/10.1103/PhysRevB.16.790 (1977).
24. Wei, S. H. & Zunger, A. Calculated natural band offsets of all II–VI and III–V semiconductors: chemical trends and the role of cation d orbitals. *Appl. Phys. Lett.* **72**, 2011. https://doi.org/10.1063/1.121249 (1998).
25. Li, Y. H. et al. Revised ab initio natural band offsets of all group IV, II-VI, and III-V semiconductors. *Appl. Phys. Lett.* **94**, 212109. https://doi.org/10.1063/1.3143626 (2009).
26. Van de Walle, C. Band lineups and deformation potentials in the model-solid theory. *Phys. Rev. B* **39**, 1871. https://doi.org/10.1103/PhysRevB.39.1871 (1989).
27. Keating, P. N. Effect of invariance requirements on the elastic strain energy of crystals with application to the diamond structure. *Phys. Rev.* **145**, 637–645. https://doi.org/10.1103/PhysRev.145.637 (1966).
28. Martin, R. M. Elastic properties of Zns structure semiconductors. *Phys. Rev. B.* **1**, 4005–4011. https://doi.org/10.1103/PhysRevB.1 (1970).
29. Lehoucq, R. B., Sorensen, D. C. & Yang, C. *ARPACK Users' Guide: Solution of large-scale Eigenvalue Problems with Implicitly Restarted Arnoldi Methods* (SIAM, 1998).
30. Slater, J. C. & Koster, G. F. Simplified Lcao method for the periodic potential problem. *Phys. Rev.* **94**, 1498–1524. https://doi.org/10.1103/PhysRev.94.1498 (1954).
31. Harrison, W. A. *Electronic Structure and the Properties of Solids* (Freeman, 1980).
32. Lee, S., Oyafuso, F., von Allmen, P. & Klimeck, G. Boundary conditions for the electronic structure of finite-extent embedded semiconductor nanostructures. *Phys. Rev. B.* **69**, 045316. https://doi.org/10.1103/PhysRevB.69.045316 (2004).

Acknowledgements

The research for this work has received funding from the European Union's Horizon 2020 Research and Innovation Programme under grant agreement no. 953183 (HARMLESS).

Author contributions

M.Z. performed the calculations and prepared the figures. A.G.-S. supervised and acquired funding for the project. Both authors worked on the manuscript.

Funding

The research for this work has received funding from the European Union's Horizon 2020 Research and Innovation Programme under grant agreement no. 953183 (HARMLESS).

Declarations

Competing interests

The authors declare no competing interests.

Additional information

Supplementary Information The online version contains supplementary material available at https://doi.org/10.1038/s41598-026-40051-2.

Correspondence and requests for materials should be addressed to M.Z. or A.G.-S.